Combination of the immersed boundary method with compact schemes for DNS of flows in complex geometry

Philippe Parnaudeau, Eric Lamballais, Dominique Heitz, Jorge Silvestrini

COMBINATION OF THE IMMERSED BOUNDARY METHOD WITH COMPACT SCHEMES FOR DNS OF FLOWS IN COMPLEX GEOMETRY

Philippe Parnaudeau[1,2], Eric Lamballais[1], Dominique Heitz[2], Jorge H. Silvestrini[3]

[1]*Laboratoire d'Etudes Aérodynamiques UMR 6609, Université de Poitiers, ENSMA, CNRS Téléport 2 - Bd. Marie et Pierre Curie B.P. 30179 86962 Futuroscope Chasseneuil Cedex, France*

[2]*Cemagref, UR TERE, 17, avenue de Cucille, CS 64427 Rennes F-35044 France*

[3]*Departamento de Engenharia Mecânica e Mecatrônica, Faculdade de Engenharia, Pontificia Universidade Catolica do Rio Grande do Sul Av. Ipiranga 6681, 90619-900 Porto Alegre - RS, Brasil*

Abstract We present a direct forcing method better suited for the use of compact finite difference schemes in Direct Numerical Simulation. The new forcing creates inside the body an artificial flow preserving the no-slip condition at the surface but reducing the step-like change of the velocity derivatives across the immersed boundary. This modification is shown to improve results both qualitatively and quantitatively for conventional and complex flow geometries.

1. CONTEXT OF THE STUDY

Despite the continual progress of computers, direct and large eddy simulation of turbulent flows in complex geometries remains a difficult task. For each flow configuration, a compromise must be specifically determined in order to correctly describe the physics of the flow for a reasonable computational cost (speed, memory requirement, code complexity). The choice of the computational grid is well known to be crucial for the determination of this compromise. In order to take accurately small details of the geometry into account, the most popular method is to generate a sophisticated grid following the body geometry, despite the fact that such grids are frequently strongly distorted, resulting in a degradation of the numerical accuracy associated with a significant increase of the global computational cost.

An alternative method to avoid the drawbacks of the body fitted approach consists in extending capabilities of codes based on simplified grids *via* the use of the 'immersed boundary method'. The basic idea of this technique is to mimic the effect of a solid surface on the fluid through a forcing applied in the body region. This operation is performed by additional terms introduced in Navier-Stokes equations. Various formulations are proposed in the literature with various names like 'virtual boundary method', 'fictitious domain method' or 'penalization method'.

Short review of immersed boundary methods. Here, we use the generic term 'immersed boundary method' introduced by [9] where this idea was employed to consider the full interaction between elastic solids and the fluid. For more simplified situations where the motion of solid surfaces is a known of the problem, three types of forcing can be distinguished: (i) feedback forcing [4], (ii) algebraic forcing [2], (iii) direct forcing [13, 3]. The feedback forcing is based on an artificial term that can 'freeze' efficiently the fluid in the body region through a damping oscillation process. The algebraic forcing is a simplified form of the feedback one where the time integral term is suppressed. With this simplification, it is possible to establish a physical analogy where the forcing can model realistically a porous medium, the limit case of a zero porosity corresponding to the modelling of a solid obstacle[1]. Unfortunately, feedback and algebraic forcings have a common drawback related to their numerical stability properties. Schematically, both methods lead to a severe additional restriction on the time step to maintain very low residual velocities in locations where no-slip conditions are expected. In order to avoid this limitation (often very expensive in terms of computational cost), the use of the direct forcing technique is very attractive. In this third method, which introduces no additional numerical stability restriction, the boundary condition is ensured in a quite straightforward way by prescribing directly the velocity in forcing region at each step of the time integration. Finally, note that it can be easily shown [7] that feedback and algebraic methods can behave asymptotically (for a 'vanishing porosity') like a forcing method when their common modelling term is time integrated with a forward (implicit) Euler scheme.

Goals of the present study. In this paper, we are interested in the strategy where the direct forcing is combined with centred finite difference schemes of high accuracy. Such a combination is *a priori* problematic due to the dis-

[1]This physical analogy can be exploited advantageously in order to interpret the meaning of the residual flow inside the modelled body (establishment of a d'Arcy law where velocity and pressure gradient are proportional) and to make easier the computation of the associated drag and lift [11]. Another advantage of this second forcing is related to its algebraic nature that offers the possibility to study theoretically its asymptotic convergence towards the case of a purely solid wall [1, 5].

continuities of the velocity derivatives created by the forcing. More precisely, the sudden application of the forcing inside the virtual boundary guarantees only the C^0 continuity of the solution whatever the spatial resolution is. The numerical code used for this study solves the incompressible Navier-Stokes equations discretized on a Cartesian collocated grid with the aid of 6^{th} order compact schemes. Despite their very favourable accuracy properties, these finite difference schemes are *a priori* not well suited for the numerical treatment of a discontinuity, even if the jump condition concerns only the first derivative. This problem is related to the quasi-spectral behaviour of compact schemes that leads to spurious oscillations in a similar way as spectral methods in presence of discontinuities (Gibbs phenomenon). In preliminary calculations based on the same numerical code as here, [7] reported that the creation of spurious oscillations in the neighbourhood of the obstacle was increased when a direct forcing was used instead of a feedback one. Since this problem was not mentioned in previous studies based on second order accurate codes [13, 3, 10], it was concluded by [7] that the spurious oscillations were a consequence of the spectral-like nature of the spatial discretization.

In this work, we propose a direct forcing method better suited for compact schemes. Basically, the idea is to create inside the body a flow preserving the no-slip condition at the surface but reducing the step-like change of the first derivative of velocities across the immersed boundary. This modification is shown to improve results both qualitatively and quantitatively.

2. FORMALISM

Schematically, the direct method consists in the application of the velocity condition $\mathbf{u}(\mathbf{x},t) = \mathbf{u_0}(\mathbf{x},t)$ in the forcing region. The target velocity field $\mathbf{u_0}(\mathbf{x},t)$ is *a priori* a known of the problem, at least at the locations where boundary conditions are expected. The discrete integration of the incompressible Navier-Stokes equations with a Δt^2 Adams-Bashforth scheme gives

$$\frac{\mathbf{u}^{n+1}-\mathbf{u}^n}{\Delta t} = \frac{3}{2}\mathbf{F}^n - \frac{1}{2}\mathbf{F}^{n-1} - \boldsymbol{\nabla}\tilde{\pi}^{n+1} + \tilde{\mathbf{f}}^{n+1} \tag{1}$$

with

$$\mathbf{F} = -\boldsymbol{\omega}\times\mathbf{u} + \nu\Delta\mathbf{u}\,, \qquad \tilde{\pi}^{n+1} = \frac{1}{\Delta t}\int_{t_n}^{t_{n+1}} \pi\, dt \tag{2}$$

where $\pi = p/\rho + \mathbf{u}.\mathbf{u}/2$ is the modified pressure (p and ρ are the pressure and the constant density respectively) while $\boldsymbol{\omega}$ is the vorticity field. The direct forcing term takes simply the expression

$$\tilde{\mathbf{f}}^{n+1} = \varepsilon\left(-\frac{3}{2}\mathbf{F}^n + \frac{1}{2}\mathbf{F}^{n-1} + \boldsymbol{\nabla}\tilde{\pi}^{n+1} + \frac{{\mathbf{u_0}}^{n+1}-\mathbf{u}^n}{\Delta t}\right) \tag{3}$$

with $\varepsilon = 1$ in the body region and $\varepsilon = 0$ everywhere else. Note that for simplicity, we consider only a motionless body surface (no time dependence of the mask function ε). In this case, the simplest method to ensure no-slip conditions is to use a zero target velocity field, namely $\mathbf{u_0} = \mathbf{0}$. As already discussed in the preceding section, this simplified forcing generates discontinuities on the first derivative of velocities that are problematic when spectral or spectral-like schemes are used. In order to avoid this difficulty, the approach proposed in this study consists in estimating a target velocity field $\mathbf{u_0}$ that allows the no-slip condition at the boundary while reducing the presence of discontinuities.

In order to do this, a first possibility is to estimate $\mathbf{u_0}$ as the reverse to the flow immediately outside the body. For instance, for a circular cylinder of diameter D, a quite natural choice for the target velocity is $\mathbf{u_0}(r, \theta, z, t) = -\mathbf{u}(D - r, \theta, z, t)$ where (r, θ, z) are cylindrical coordinates associated to the circular body geometry. This type of forcing has already been tested by previous authors [13, 3] but only for the prescription of the inner velocities at the closest grid points to the body surface. In the present context of compact schemes, such a selective action would not be efficient enough due to the non-local character of the derivative estimation. Then, we define a target velocity in the full body domain as

$$\mathbf{u_0}(r, \theta, z, t) = -f(r)\mathbf{u}(D - r, \theta, z, t) \tag{4}$$

where the modulation function

$$f(r) = \sin(2\pi r^2/D^2) \tag{5}$$

is adjusted to ensure the regularity of inner velocities and to avoid the singularity at $r = 0$. Naturally, other choices of $f(r)$ are possible provided that the three following conditions are verified (i) $f(1/2) = 1$: accurate reverse condition near the body surface, (ii) $f(0) = 0$: singularity cancellation and (iii) $0 \leq f(r) \leq 1$ with moderate first and second derivatives for $0 \leq r \leq 1/2$. For instance, $f(r) = \frac{1}{2}[1 - \cos(2\pi r/D)]$ is another suitable modulation function. Here, we choose the expression (5) because it cancels slightly more rapidly the target velocity when $r \to 0$, but it should be recognized that this choice is a partly arbitrary.

Another point is that it is possible to apply the reverse condition only to the tangential component of the velocity, the normal component being simply cancelled. Such a forcing leads to concentric streamlines inside the cylinder. Note this cancellation of the normal velocity inside the body does not create additional discontinuities due to the incompressibility condition at the boundary that guaranties a zero normal derivative for this velocity component. In preliminary calculations (not presented here), we observed that both treatments of the internal normal velocity (reverse condition or cancellation) lead to equivalent results. In the data presented in the following, the normal inner velocity was

maintained to zero except for the case of the tapered cylinder where the reverse condition was directly applied at the vectorial level. In complex geometry, the reverse condition is easier to implement because no projection of the velocity vectors is necessary in order to distinguish normal and tangential components. Naturally, the estimation of the target velocity using (4) on a Cartesian grid needs to perform interpolations. Here, we only use a multilinear interpolation to prescribe the internal flow from the knowledge of the external one. Despite the second order accuracy of such a procedure (which is significantly lower than to the formal accuracy of the numerical code itself), it will be shown in the following that important benefits can be obtained from the use of 6^{th} order compact schemes.

An important point is that the target velocity field is not *a priori* divergence free. For this reason, the verification of the incompressible condition $\boldsymbol{\nabla}.\mathbf{u}^{n+1} = 0$ must be discarded inside the body by allowing a mass source/sink in region where $\varepsilon = 1$. Following the approaches proposed by [13, 6], a first possibility is to impose $\boldsymbol{\nabla}.\mathbf{u}^{n+1} = \varepsilon\ \boldsymbol{\nabla}.{\mathbf{u_0}}^{n+1}$. Here, we use a slightly modified condition $\boldsymbol{\nabla}.\mathbf{u}^{n+1} = \boldsymbol{\nabla}.\left(\varepsilon{\mathbf{u_0}}^{n+1}\right)$ that was found to reduce more efficiently oscillations in the vicinity of the obstacle.

In the framework of the fractional step method, several adjustments are necessary in order to eliminate the various couplings introduced by the forcing method. In this context, a three step advancement yields

$$\frac{\mathbf{u}^* - \mathbf{u}^n}{\Delta t} = \frac{3}{2}\mathbf{F}^n - \frac{1}{2}\mathbf{F}^{n-1} - \boldsymbol{\nabla}\tilde{\pi}^n + \tilde{\mathbf{f}}^* \tag{6}$$

$$\frac{\mathbf{u}^{**} - \mathbf{u}^*}{\Delta t} = \boldsymbol{\nabla}\tilde{\pi}^n \tag{7}$$

$$\frac{\mathbf{u}^{n+1} - \mathbf{u}^{**}}{\Delta t} = -\boldsymbol{\nabla}\tilde{\pi}^{n+1} \tag{8}$$

with the associated forcing term

$$\tilde{\mathbf{f}}^* = \varepsilon\left(-\frac{3}{2}\mathbf{F}^n + \frac{1}{2}\mathbf{F}^{n-1} + \boldsymbol{\nabla}\tilde{\pi}^n + \frac{{\mathbf{u_0}}^{n+1} - \mathbf{u}^n}{\Delta t}\right) \tag{9}$$

where the target velocity ${\mathbf{u_0}}^{n+1}$ is estimated by

$${\mathbf{u_0}}^{n+1}(r,\theta,z,t) = -f(r)\mathbf{u}^*(D - r,\theta,z,t) \tag{10}$$

In first analysis, it can be expected that the splitting error introduced by the use of $\tilde{\mathbf{f}}^*$ in (6) and $\mathbf{u}^*$ in (10) instead of $\tilde{\mathbf{f}}^{n+1}$ and $\mathbf{u}^{n+1}$ respectively is only Δt^2 without any consequence on the final order of the time advancement.

The last step is to derive a Poisson equation compatible with the condition $\boldsymbol{\nabla}.\mathbf{u}^{n+1} = \boldsymbol{\nabla}.\left(\varepsilon{\mathbf{u_0}}^{n+1}\right)$. Here, we propose to use the approximation

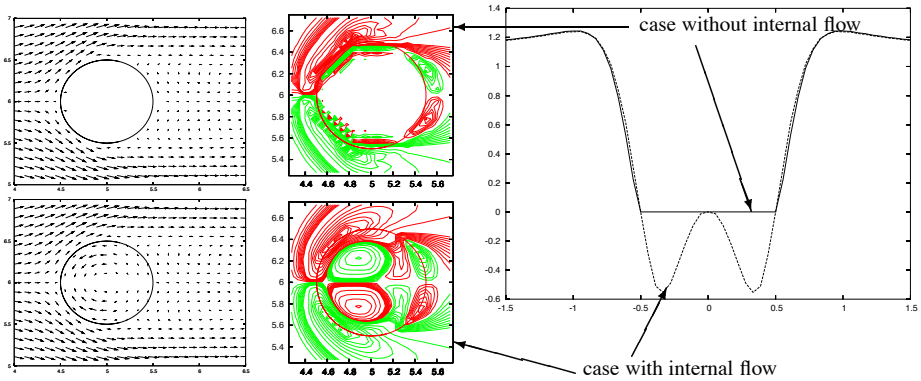

(a) Velocity field plots (b) Vorticity plots (c) Velocity profiles $u_x(x_{cyl} = 5D, y)$

Figure 1. Comparison between two direct forcing methods with and without internal flow at $Re = 40$. The computational domain $(L_x, L_z) = (20D, 12D)$ is discretized on $n_x \times n_z = 361 \times 217$ grid points and the numerical code is based on Δx^6 compact schemes.

$\boldsymbol{\nabla}.\left(\varepsilon \mathbf{u_0}^{n+1}\right) = \boldsymbol{\nabla}.\left(\varepsilon \mathbf{u}^{**}\right)$ that leads to the pressure equation

$$\boldsymbol{\nabla}.\boldsymbol{\nabla}\tilde{\pi}^{n+1} = \frac{\boldsymbol{\nabla}.\left[(1-\varepsilon)\mathbf{u}^{**}\right]}{\Delta t} \tag{11}$$

where the conventional Poisson equation is recovered for $\varepsilon = 0$ whereas inside the body, the condition $\varepsilon = 1$ yields the Laplace equation. Note that other variations on the method are possible, especially concerning the correction step (8) that can be conditioned by ε as in [13] where the pressure cells are explicitly masked (in this case, a two step splitting is only necessary). In this work, the correction by pressure gradients is performed everywhere in the computational domain *via* a fractional method in three steps.

3. RESULTS

Steady 2D wake at $Re = 40$. The benefit of the use of a non-zero target velocity is shown in figure 1 where a constant flow around a 2D cylinder is considered. Two cases are compared depending on the target velocity treatment that can be zero (no internal flow) or given by (4) for the tangential component. The comparison between both forcing methods shows clearly the improvement offered by the use of a reverse flow inside the body. First, the examination of the longitudinal velocity profiles (1c view) obtained in each case shows clearly the more realistic near-body behaviour of the velocity when the first derivative discontinuity is avoided. The improvement of the near-body data is confirmed by the examination of vorticity isocontours (1b view). Note in particular the reduction of spurious vorticity when a reverse flow is imposed

Table 1. Comparison of statistical results obtained from various combinations between the forcing method and the numerical code accuracy. All DNS are performed using a computational domain $(L_x, L_y, L_z) = (20D, 2\pi D, 12D)$ discretized on $n_x \times n_y \times n_z = 361 \times 48 \times 216$ grid points. Data of DNS II' are from [7]. The streamwise location of the cylinder is $x_{cyl} = 5D$.

DNS	*I*	*II*	*III*	*IV*	*II'*
Forcing method	direct	direct	direct	direct	feedback
Internal flow	yes	no	yes	no	no
Scheme accuracy	Δx^6	Δx^6	Δx^2	Δx^2	Δx^6
Strouhal number	0.206	0.196	0.211	0.213	0.20
$L_{R_{xx}}/D$	1.38	1.55	1.22	1.27	1.64
Max$[R_{xx}]/U^2$	0.26	0.20	0.32	0.31	0.19

inside the cylinder. Quantitatively, by comparison to previous [14] or highly resolved results, we observe that the characteristic length scales of the flow are predicted more accurately when using the new forcing with the present spatial resolution. For instance, we verified that this new method allows a satisfactory prediction of the length of the wake bubble that is $L_w = 2.30D$ ($\pm 0.03D$), in good agreement with [14] who found $L_w = 2.27D$. In contrast, the use of a zero target velocity field leads to an overestimation of 10%, i.e., $L_w = 2.50D$ ($\pm 0.03D$). Finally, note that we have verified that both forcing methods allow the convergence towards the correct length of the wake bubble while reducing considerably the spurious vorticity in the neighbourhood of the cylinder.

Unsteady 3D wake at $Re = 300$. In this section, we compare four DNS combining three different forcing methods with two numerical codes based on Δx^2 or Δx^6 (compact) centred finite difference schemes (see table 1 and its caption for more details about the simulation parameters). Concerning the length scale selection, similar trends as for $Re = 40$ are recovered for this unsteady case at higher Reynolds number. The formation length $L_{R_{xx}}$ (deduced from the streamwise location where the Reynolds stress R_{xx} reaches its maximum) is better predicted using the forcing (4) whereas the use of $\mathbf{u_0} = \mathbf{0}$ leads to a typical 10% overestimation, in agreement with previous observations of [7] based on DNS using the feedback forcing method. Compared to reference values, an improvement of the Strouhal number prediction is also obtained. However, the comparison between DNS III and IV shows that these improvements are not obtained when Δx^2 schemes are used, this insensitivity to the forcing method (with or without internal flow) being consistent with the previous observations of [3]. Present conclusions can be confirmed by the examination of $\langle u_x \rangle$ and R_{xx} profiles presented in figure 2 for each case. The improvement offered by the use of Δx^6 compact schemes is clearly shown,

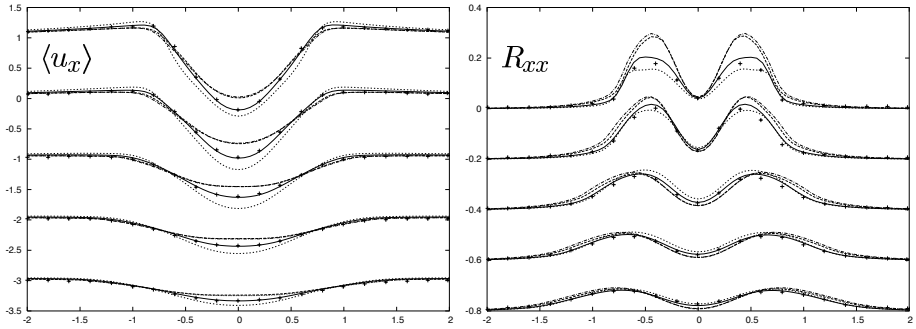

Figure 2. Profiles of longitudinal velocity statistics at different streamwise locations $(x - x_{cyl})/D = 1.2, 1.5, 2.0, 2.5, 3.0$. — : DNS I; ·····: DNS II; _ _ _ _: DNS III; _ . _ . : DNS IV; +: reference data obtained by spectral DNS based on a cylindrical grid [8].

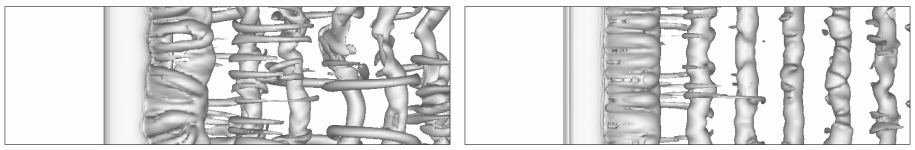

Figure 3. Isosurfaces of vorticity modulus $\omega = 1.5U_c/D$. Left: DNS I, right: DNS III.

especially when the forcing with internal flow is applied (DNS I). Conversely, the overestimation of the longitudinal velocity fluctuations obtained for both DNS III and IV emphasizes the interest of the use of highly accurate schemes, even if the formal accuracy is significantly lower due to the forcing method itself. Note that this present overestimation is in agreement with the results of [10] who used also a numerical code based on Δx^2 schemes. Physically, at marginal resolution, the combination of Δx^2 schemes with a direct forcing method seems to inhibit the 3D motions near the cylinder. This phenomenon can be shown not only by statistical results but also through instantaneous visualizations. For instance, figure 3 presents a comparison between isosurfaces of vorticity modulus obtained from DNS I and III. The artificial inhibition of 3D motions in DNS III is clearly confirmed, especially through the lack of longitudinal vortices (stretched between the Karman structures) compared to results from DNS I.

Unsteady 3D wakes in complex geometry. In this section, two specific wake configurations are compared (see the caption of figure 4 for details about simulation parameters). The case A corresponds to a flow of constant velocity $U = U_c$ over a tapered cylinder with a diameter $D(y)$ ranging from

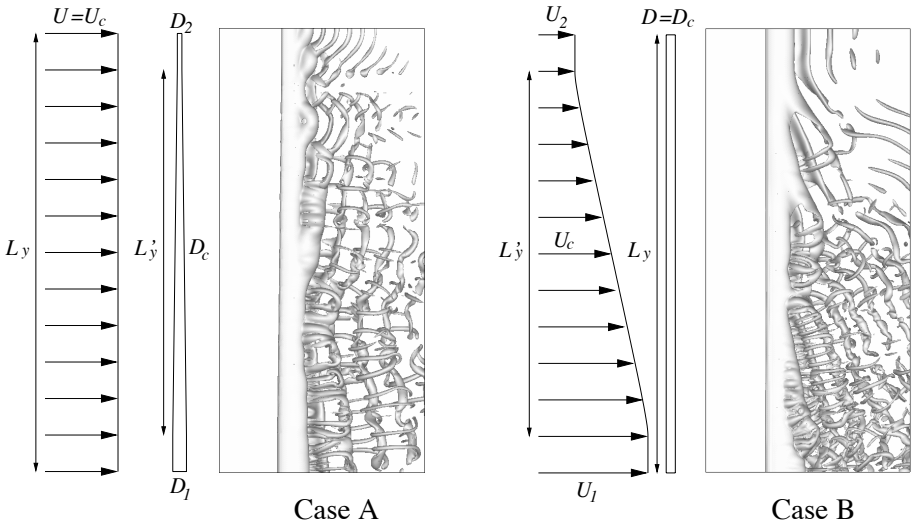

Figure 4. Comparison of instantaneous vorticity visualizations. The computational domain $(L_x, L_y, L_z) = (22D_c, 48D_c, 12D_c)$ is discretized on $n_x \times n_y \times n_z = 397 \times 385 \times 216$ grid points with $L'_y = 40D_c$ and $x_{cyl} = 7D$. Data of Case B are from [12] who used a feedback forcing method.

$D_2 = D_c/2$ to $D_1 = 3D_c/2$. The case B consists in a shear flow ($U_2 < U(y) < U_1$ with $U_2 = U_c/2$ and $U_1 = 3U_c/2$) over a cylinder of constant diameter $D = D_c$. For each case, $D(y)$ or $U(y)$ vary linearly from $y = -L'_y/2$ to $y = L'_y/2$ (see figure 4) and the common Reynolds number $Re_c = U_c D_c/\nu$ is 200. Hence, both flow configurations cover an equivalent range of local Reynolds number $Re = UD/\nu$ with $100 < Re < 300$. Moreover, in both cases, a local adjustment of the vortex shedding frequency f on the local diameter $D(y)$ or velocity $U(y)$ can be expected by limiting (in first analysis) the deviation of the local Strouhal number $St = fD/U$ from its value for a conventional wake. Note that such a local selection leads to high frequencies in the low Re region for case A and the opposite situation for case B. Naturally, this selection cannot be purely local due to the preservation of the coherence of the flow motion in y-direction. The vortical organization obtained for each case is presented in figure 4. Despite the similarities between these two flow configurations, the local mechanisms of vortex shedding lead to the formation of well marked cells in case A whereas in case B, the main effects are linked to the selection of oblique structures (note however that a cellular pattern of vortex shedding can also be identified for case B by means of a frequency analysis [12]). The occurrence of dislocations (phase breaking, tearing of vortices) can be observed in both cases, but these phenomena are found to be more frequent

for case A. A quantitative comparison between these two flows (frequency analysis, mean and fluctuating motions) is currently in progress.

Acknowledgments

Calculations were carried out at the IDRIS. This study was partially supported by the Région Poitou-Charentes and the CNRS.

References

[1] P. Angot, C.-H. Bruneau, and P. Fabrie. A penalization method to take into account obstacles in incompressible viscous flows. *Numer. Math.*, **81**:497–520, 1999.

[2] E. Arquis and J. P. Caltagirone. Sur les conditions hydrodynamiques au voisinage d'une interface milieu fluide-milieu poreux : application à la convection naturelle. *C. R. Acad. Sci.*, **299**(1):1–4, 1984. Serie II.

[3] E. A. Fadlun, R. Verzico, P. Orlandi, and J. Mohd-Yusof. Combined immersed-boundary finite-difference methods for three-dimensional complex flow simulations. *J. Comp. Phys.*, **161**:35–60, 2000.

[4] D. Goldstein, R. Handler, and L. Sirovich. Modeling a no-slip boundary condition with an external force field. *J. Comp. Phys.*, **105**:354–366, 1993.

[5] N. K.-R. Kevlahan and J.-M. Ghidaglia. Computation of turbulent flow past an array of cylinders using a spectral method with brinkman penalization. *Eur. J. Mech. B/Fluids*, **20**:333–350, 2001.

[6] J. Kim, D. Kim, and H. Choi. An immersed-boundary finite-volume method for simulations of flow in complex geometries. *J. Comp. Phys.*, **171**:132–150, 2001.

[7] E. Lamballais and J. Silvestrini. Direct numerical simulation of interactions between a mixing layer and a wake around a cylinder. *J. Turbulence*, 3:028, 2002.

[8] R. Mittal and S. Balachandar. On the inclusion of three-dimensional effects in simulations of two-dimensional bluff-body wake flows. In *Proc. of ASME Fluids engineering division summer meeting*, Vancouver, British Columbia, Canada, 1997.

[9] C. S. Peskin. Flow patterns around heart valves: a numerical method. *J. Comp. Phys.*, **10**:252–271, 1972.

[10] U. Piomelli and E. Balaras. Numerical simulations using the immersed boundary technique. In *Proc. third AFSOR International Conference on Direct and Large-Eddy Simulations*, Arlington, Texas, USA, 2002.

[11] K. Schneider and M. Farge. Adaptative wavelet simulation of a flow around an impulsively started cylinder using penalisation. *Appl. Comput. Harmon. Anal.*, **12**:374–380, 2002.

[12] J. Silvestrini and E. Lamballais. Direct numerical simulation of oblique vortex shedding from a cylinder in shear flow. In *Proc. 3^{rd} International Symposium on Turbulence and Shear Flow Phenomena*, Sendai, Japan, 2003.

[13] F. Tremblay, M. Manhart, and R. Friedrich. DNS of flow around a circular cylinder at a subcritical reynolds number with cartesian grid. In *Proc. of the 8th European Turbulence Conference, EUROMECH*, Barcelona, Spain, 2000.

[14] T. Ye, R. Mittal, H. S. Udaykumar, and W. Shyy. An accurate cartesian grid method for viscous incompressible flow with complex immersed boundaries. *J. Comp. Phys.*, **156**:209–240, 1999.